The Ho_2MnRuO_7 pyrochlore oxide: Magnetic structure versus magnetic frustration

Cite as: J. Appl. Phys. **107**, 093919 (2010); https://doi.org/10.1063/1.3393994
Submitted: 28 October 2009 • Accepted: 19 March 2010 • Published Online: 07 May 2010

M. Retuerto, M. J. Martínez-Lope, C. de la Calle, et al.

The Ho_2MnRuO_7 pyrochlore oxide: Magnetic structure versus magnetic frustration

M. Retuerto,[1,a)] M. J. Martínez-Lope,[1] C. de la Calle,[1] R. Martínez-Coronado,[1] M. García-Hernández,[1] J. A. Alonso,[1] and M. T. Fernández-Díaz[2]
[1]*Instituto de Ciencia de Materiales de Madrid, CSIC, Cantoblanco, E-28049 Madrid, Spain*
[2]*Institut Laue Langevin, BP 156X, Grenoble F-38042, France*

(Received 28 October 2009; accepted 19 March 2010; published online 7 May 2010)

A pyrochlore-like phase of composition Ho_2MnRuO_7 has been synthesized by a soft-chemistry procedure followed by thermal treatments at moderate temperatures up to 900 °C for 12 h in air. It has been characterized by x-ray diffraction and neutron powder diffraction (NPD), as well as dc and ac susceptibilities. As in the parent $Ho_2Mn_2O_7$ oxide, the magnetic Mn and Ru ions statistically occupy the 16*c* sites in a cubic unit cell with space group $Fd\bar{3}m$, which define a potentially frustrated three-dimensional array of corner sharing $(Mn,Ru)_4$ tetrahedra. The dc and ac magnetic susceptibilities of Ho_2MnRuO_7 display a sharp increase near 60 K. In addition, the field-cooled and zero-field-cooled curves diverge below 30 K. The ac data present frequency variability below 60 K and broad frequency dependent maxima at lower temperatures (~30 K), suggesting a spin-glass like behavior similar to $Ho_2Mn_2O_7$. However, a low-temperature NPD study of the magnetic structure unveils an antiferromagnetic coupling of two subsets of Mn^{4+}/Ru^{4+} spins, indicating that the magnetic frustration is partially relieved by the random distribution of Mn and Ru over the 16*c* sites; at lower temperatures there is a polarization of the Ho^{3+} magnetic moments, which also participate in the magnetic structure. Under an external magnetic field the Ho moments become totally polarized, giving a saturation magnetization at 2 K of 10.8 μ_B/f.u. at 5 T. © *2010 American Institute of Physics*. [doi:10.1063/1.3393994]

I. INTRODUCTION

Pyrochlore materials have attracted considerable attention due to their wide spectrum of potential applications associated with their electrical, magnetic, dielectric, optical, or catalytic properties.[1] These properties are controlled by the ionic size, the electronic configuration, and the polarizability of the ions or the synthesis conditions. Pyrochlore oxides have the composition $A_2B_2O_7$ and, in general, crystallize in the cubic, face-centered space group $Fd\bar{3}m$,[1] where the A cations are eightfold coordinated, located within scalenohedra (distorted cubes) that contains six equally spaced oxygen anions (O1) and two additional oxygen anions (O2) at a slightly shorter distance from the central cations. The smaller B cations are sixfold coordinated in trigonal antiprisms (distorted octahedra) with all the six oxygen anions (O1) at equal distance of the central cation.

The interest in Mn-pyrochlores was triggered by the discovery of colossal magnetoresistance (CMR) in $Tl_2Mn_2O_7$ (Refs. 2–4) and the description of different doped derivatives.[5–8] It was the first time that CMR was reported in manganese oxides without Mn-mixed valence. $Tl_2Mn_2O_7$ is a ferromagnetic (FM) material with $T_C=142$ K and a saturated magnetic moment at 5 K of 2.59 μ_B per Mn ion. This oxide displays a metallic behavior for the high temperature state; the resistivity exhibits a peak at T_C, together with a one-order of magnitude drop below T_C. There is no structural anomaly associated with the change in the magnetotransport properties at T_C.[3] The CMR effect in $Tl_2Mn_2O_7$ is ascribed to the strong scattering of the conduction electrons by spin fluctuations associated with the FM ordering of the Mn sublattice.[4]

These exotic properties are only observed in the Tl compound, due to the strong hybridization of the voluminous Tl (6*s*) orbitals with O (2*p*) and Mn (3*d*) orbitals.[9] However, the magnetic interactions are much weaker when Tl is replaced by a rare earth ion (R^{3+}). $R_2Mn_2O_7$ pyrochlores are isostructural with the Tl compound[10,11] but they are FM semiconductors with much lower T_C.[10,12] The FM superexchange interactions take place across the rather bent Mn–O–Mn bond angles of ~130° characteristic of the B_2O_6 framework of the pyrochlore structure, that allows a crossover from 180° antiferromagnetic (AFM) interactions to 90° FM interactions.[13] A detailed study based on several complementary experimental techniques has revealed that the magnetism of $R_2Mn_2O_7$ pyrochlores is of spin-glass type at low temperatures.[14,15]

Aiming to introduce novel magnetic interactions in Mn-based pyrochlore oxides we have prepared a new pyrochlore-type Ho_2MnRuO_7 oxide, where the Mn sublattice has been half-replaced by Ru cations. In fact, previous studies on closely related Ru-containing pyrochlore oxides in the series $R_2Ru_2O_7$ (R=Y, Nd, and Ho) revealed that the Ru^{4+} moments are ordered at higher temperatures (T~100 K) than $R_2Mn_2O_7$ pyrochlores.[16,17] The compound $Ho_2Ru_2O_7$, previously reported, presents very attractive magnetic properties related to some kind of spin-ice state.[17,18] In addition, there

a)Author to whom correspondence should be addressed. Electronic mail: mretuerto@icmm.csic.es.

are other pyrochlores that present very interesting magnetic behavior as the dipolar spin-ice ground state found for $Ho_2Ti_2O_7$ below 2 K.[19]

In this work, we describe a comprehensive study of the crystal structure and magnetism of Ho_2MnRuO_7 from neutron powder diffraction (NPD) data, in complement with dc and ac magnetic susceptibilities.

II. EXPERIMENT

A. Sample preparation

Ho_2MnRuO_7 was prepared by a wet chemistry procedure involving metal citrates. This method requires the formation of very reactive precursors starting from an aqueous solution of the metal ions and citric acid. Stoichiometric amounts of Ho_2O_3, $MnCO_3$, and RuO_2 were solved in citric acid and some drops of nitric acid, and the solution was slowly evaporated, leading to organic resins that contain a homogeneous distribution of the involved cations. The formed resins were dried at 120 °C, decomposed at 600 °C for 12 h, and the organic materials and the nitrates were eliminated in a subsequent treatment at 800 °C in air, for 2 h. This treatment gave rise to finely divided and homogeneous precursor materials that finally were heated in air at 900 °C for 12 h to obtain the pure pyrochlore oxide phase.

B. X-ray diffraction (XRD) and neutron diffraction data

The initial characterization of the product was carried out by XRD using a Bruker-axs D8 diffractometer (40 kV, 30 mA), controlled by a DIFFRACTPLUS software, in Bragg–Brentano reflection geometry with Cu K_α radiation ($\lambda = 1.5418$ Å) and a position sensitive detector (PSD). A filter of nickel allowed the complete removal of Cu K_β radiation. The slit system was selected to ensure that the x-ray beam was completely within the sample at all angles of 2θ. For the structural refinement NPD experiments were carried out in the high-resolution powder diffractometer D1A ($\lambda = 1.91$ Å) at the ILL in Grenoble. The patterns were collected in a displex unit at room temperature (RT), 50, 10, and 2 K. About 2 g of sample were contained in a vanadium can; a time of 3 h was required to collect a full diffraction pattern. The NPD data were analyzed by the Rietveld method[20] using the FULLPROF program.[21] A pseudo-Voigt function was chosen to generate the line shape of the diffraction peaks. The following parameters were refined in the final run: scale factor, background coefficients, zero-point error, pseudo-Voigt corrected for asymmetry parameters, positional coordinates, and isotropic thermal factors for all the atoms. The neutron scattering lengths for Ho, Ru Mn, and O are 8.44 fm, 7.02 fm, −3.75 fm, and 5.80 fm, respectively.[21]

C. dc and ac magnetic susceptibilities

The magnetic measurements were performed in a commercial superconducting quantum interference device magnetometer. The dc susceptibility was measured under a 0.1 T magnetic field in the temperature interval $2 < T < 400$ K. Isothermal magnetization curves were obtained for magnetic fields going from −5 T to 5 T at T=2, 10, and 30 K. ac magnetic susceptibility measurements were carried out in a physical property measurement system (PPMS) device for temperatures form 2 to 70 K. The frequencies for the transversal oscillating magnetic field were 30, 100, 300, 600, 900, 3000, and 9000 Hz.

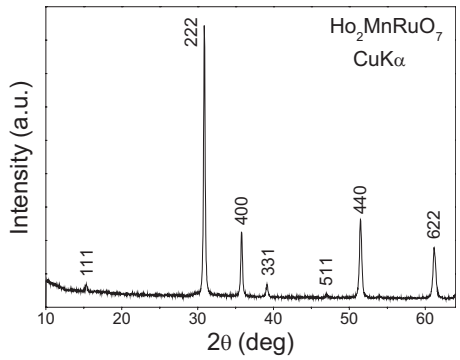

FIG. 1. XRD pattern of Ho_2MnRuO_7, indexed in a cubic unit cell with parameter a=10.049(1) Å.

III. RESULTS

A. Crystal structure

Ho_2MnRuO_7 was obtained as a black, well-crystallized polycrystalline sample. The XRD diagram is characteristic of a pyrochlore-type structure of formula $A_2B_2O_7$ (Fig. 1), indexed in a cubic, face-centered unit cell of parameter a =10.049(1) Å. No impurity phases were detected. To carry out a more accurate structural study of Ho_2MnRuO_7, we performed a NPD investigation at RT, 50, 10, and 2 K. The NPD patterns were all fully refined in a cubic unit cell with lattice parameter around 10 Å. As mentioned in the introduction, the crystal structure of Ho_2MnRuO_7 is defined in the cubic $Fd\bar{3}m$ space group, with origin at (1/8, 1/8, 1/8). In this setting the Ho cations are located at 16*d* (1/2,1/2,1/2) sites, the Mn and Ru cations are placed at 16*c* (0,0,0) positions and the two kinds of nonequivalent oxygen atoms (O1 and O2) at 48*f* (x, 1/8, 1/8) and 8*b* (3/8, 3/8, 3/8) sites, respectively. Table I summarizes the unit-cell, atomic, and thermal parameters and discrepancy factors after the Rietveld refinements at the different temperatures. Table II contains the main interatomic distances and angles. Figure 2(a) illustrates the good agreement between the observed and calculated NPD patterns at RT. The first series of Bragg reflections corresponds to the crystallographic reflections and the second series corresponds to vanadium from the sample holder. The neutron diffraction pattern collected at T=2 K contains additional information from magnetic origin. Extra peaks and additional intensity on the low-angle Bragg reflections is attributed to the establishment of a long-range ordered magnetic structure. Figure 2(b) illustrates the Rietveld refinement of the NPD pattern at 2 K, the second series of Bragg reflections corresponds to vanadium from the sample holder and the third series to the magnetic reflections. The determination of the magnetic structure is described below.

In the $A_2B_2O_7$ pyrochlore structure, the A and B cations can undergo some antisite disordering in partially disordered

TABLE I. Unit-cell, positional, thermal parameters, and ordered magnetic moments for Ho_2MnRuO_7 in cubic $Fd\bar{3}m$ (no. 227) space group, from NPD data at 295, 50, 10, and 2K. Ho are placed at 16*d* (1/2, 1/2, 1/2), Mn/Ru at 16*c* (0, 0, 0), O1 at 48*f* (x, 1/8, 1/8), O2 at 8*b* (3/8, 3/8, 3/8) positions.

Temperature (K)	295	50	10	2
a (Å)	10.0491(2)	10.0369(2)	10.0368(2)	10.0366(2)
V (Å^3)	1014.79(3)	1011.10(3)	1011.07(4)	1011.02(3)
Ho				
B (Å^2)	0.36(5)	0.15(4)	0.19(4)	0.16(2)
(Mn/Ru)				
B (Å^2)	0.6(1)	0.1(1)	0.4(1)	0.2(1)
O1				
x	0.3316(1)	0.3319(1)	0.3319(1)	0.3320(2)
B (Å^2)	0.72(4)	0.41(3)	0.55(4)	0.48(3)
O2				
B (Å^2)	0.65(7)	0.37(7)	0.57(8)	0.47(7)
Magnetic moment Mn (μ_B)			1.69(9)	2.33(7)
Magnetic moment Ho (μ_B)			1.3(1)	1.82(8)
Reliability factors				
χ^2	1.66	1.31	1.35	2.05
R_p (%)	3.07	3.38	3.4	3.47
R_{wp} (%)	4.22	4.30	4.35	4.39
R_{exp} (%)	3.08	3.76	3.74	3.07
R_{mag} (%)			23.1	22.9
R_I (%)	2.71	3.09	3.26	3.64

structures. The long-range order occurs when they differ significantly in ionic radii, at least for radius ratio $r_A/r_B > 1.46$, for smaller ratios they present a disordered CaF_2 structure. In Ho_2MnRuO_7, we can estimate the radius ratio $r(Ho^{3+})/r(Mn^{4+}/Ru^{4+})$ as 1.76, for $r(^{VIII}Ho^{3+})=1.015$ Å, $r(^{VI}Mn^{4+})=0.53$ Å, and $r(^{VI}Ru^{4+})=0.62$ Å,[22] theoretically indicating a full A/B ordering. Moreover, by NPD we could experimentally determine the degree of order between Ho and Mn/Ru cations over the A and B sites: the refinement indicates a full order with an excellent fit to the data. However, Mn and Ru cations are completely disordered over the B positions of the structure. An analysis of the possible oxygen vacancies on either 48*f* or 8*b* positions was also feasible, given the visibility of oxygen atoms by neutrons. After the refinement of the occupancy factors for O1 and O2, no oxygen vacancies were detected within the standard deviations.

B. dc and ac susceptibilities

The dc susceptibility versus temperature data, displayed in Fig. 3, show an abrupt increase of χ suggesting the onset of magnetic ordering at $T \sim 65$ K. The ZFC and FC curves, which overlap at high temperatures, diverge on decreasing the temperature below 30 K.

The reciprocal magnetic FC susceptibility shows a slight curvature immediately above T_C but it is almost linear in the temperature range from 200 to 400 K. In this temperature interval, the inverse of the susceptibility follows the Curie–Weiss law, as shown in the inset of Fig. 3. An effective paramagnetic moment of $\mu_{eff}=15.69(1)$ μ_B/f.u. and a Weiss temperature of $\theta_W=-22.91(8)$ K were determined from the Curie–Weiss fit. This is indicative of weak AFM interactions on this compound. The magnetic response is due to Ho, Mn, and Ru paramagnetic moments. An estimation of the theoretical effective magnetic moment can be gained by considering the expression $\mu_{eff}=[2\mu_B(Ho^{3+})^2+\mu_B(Mn^{4+})^2+\mu_B(Ru^{4+})^2]^{1/2}$. The effective magnetic moments for Mn^{4+}, Ru^{4+}, and Ho^{3+} ($^5I_8$ ground state configuration) are 3.87 μ_B, 2.83 μ_B, and 10.60 μ_B, respectively, that means an effective magnetic moment of 15.74 μ_B, in excellent agreement with the experimental value.

TABLE II. Selected atomic distances (Å) and angles (deg) for Ho_2MnRuO_7 at 295, 50, 10, and 2K.

Temperature (K)	295	50	10	2
Ho-O1(x6)	2.4533(7)	2.4486(8)	2.4484(8)	2.4477(8)
Ho-O2(x2)	2.17569(2)	2.17305(2)	2.17301(3)	2.17294(3)
Mn/Ru-O1(x6)	1.9566(7)	1.9554(7)	1.9554(8)	1.9557(9)
Ho-O1-Ho	92.79(3)	92.88(3)	92.88(3)	92.91(4)
Ho-O2-Ho	109.47	109.47	109.47	109.47
Mn/Ru-O1-Mn/Ru	130.43(2)	130.29(2)	130.28(3)	130.24(3)

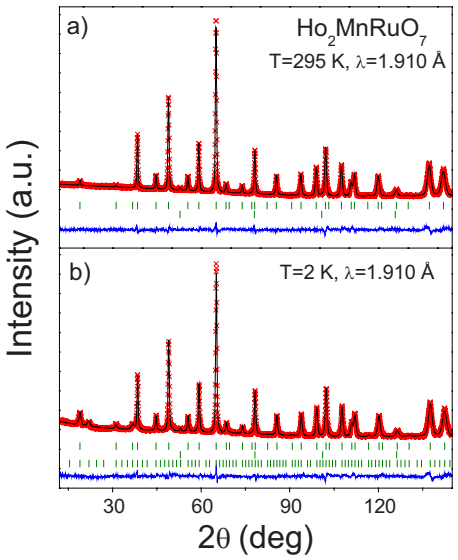

FIG. 2. (Color online) Comparison of the observed (crosses), calculated (solid line), and difference (at the bottom) NPD patterns. (a) T=295 K. The two series of tick marks correspond to the positions of the allowed Bragg reflections for the main phase and vanadium. (b) T=2 K. The third series of tick marks corresponds to the magnetic reflections.

The isothermal magnetization curves measured at 2, 10, and 30 K are displayed in Fig. 4. A narrow hysteresis loop is observed at T=2 K characteristic of a FM order. The curve shows a remnant magnetization of 2.1 μ_B per formula unit and a maximum magnetization of 10.8 μ_B/f.u., reached for the maximum applied field of 5 T. At 10 K, the curve is still characteristic of a ferromagnet with a remnant magnetization of 0.8 μ_B and a maximum magnetization of 10.4 μ_B/f.u. at 5 T. However, at T=30 K the curve merely presents a very weak FM component.

The thermal evolution of the ac susceptibility is shown in Fig. 5 for temperatures ranging from 2–70 K at different frequencies (f) varying from 30 to 9000 Hz. χ' and χ'' represent, respectively, the real (in-phase) and imaginary (out-of-phase) components of the susceptibility. Both χ' and χ'' show a sharp increase at T≈60 K in accordance with the long-range magnetic ordering temperature determined by the dc susceptibility measurement. However, another peak is observed a few degrees below, at around 30–35 K. This second anomaly is frequency dependent in both χ' and χ'' curves.

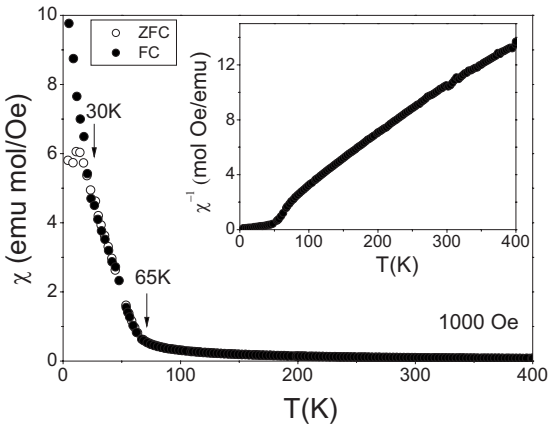

FIG. 3. Thermal evolution of the FC and ZFC dc susceptibility. Upper inset: reciprocal susceptibility (FC data).

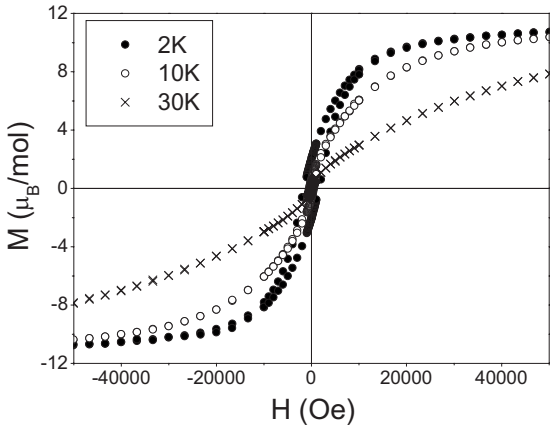

FIG. 4. Magnetization vs magnetic field isotherms at T=2, 10, and 30 K.

C. Determination of the magnetic structure

Figure 6 shows the temperature dependence of the low-angle region of the neutron diffraction patterns of Ho_2MnRuO_7 measured at 2, 10, 50, and 300 K. The low-angle reflections, typically (111), increase in intensity at 10 and 2 K. Additionally, there is a magnetic contribution on the (002) peak that totally vanishes at 50 and 300 K. This reflection is forbidden by the face-centered symmetry of the $Fd\bar{3}m$ space group but it can be indexed in a primitive unit cell with the same lattice parameter $\mathbf{a}\approx 10$ Å. As the size of the magnetic and crystallographic unit cell is coincident, the propagation vector is $\mathbf{k}=0$. The magnetic structure has been determined from the 2 K data. A satisfactory solution was found by modeling a collinear AFM coupling between Mn/Ru cations at the B sublattice, in fact, this sublattice is splitted in two subsets of Mn/Ru moments antiferromagnetically

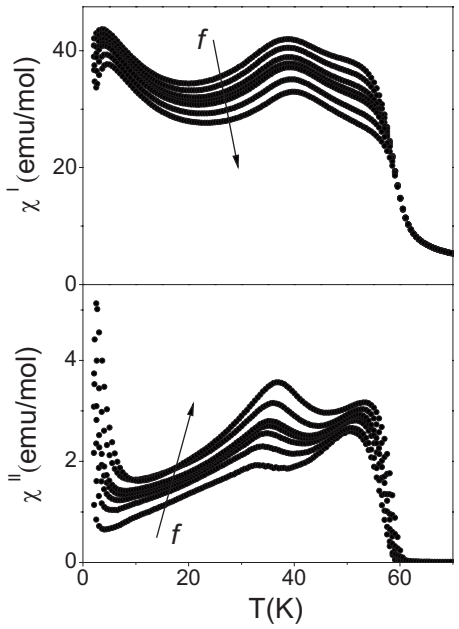

FIG. 5. Thermal evolution of the real an imaginary part of the ac susceptiblity.

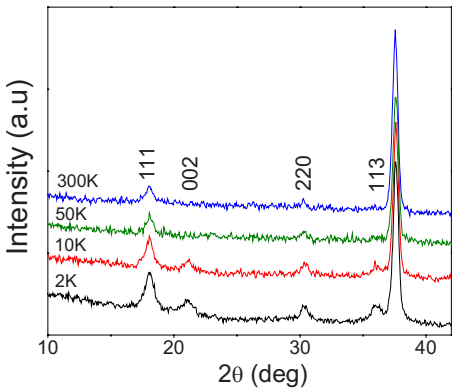

FIG. 6. (Color online) Thermal evolution of the NPD patterns measured at 2, 10, 50, and 300 K.

coupled to each other. This splitting breaks the face centering of the magnetic lattice and accounts for the magnetic intensity on the (002) reflection. The refined magnetic moments were considered to be oriented along the [001] axis since in a cubic system it is not possible to determine their orientation. This arrangement would define an intrinsically frustrated magnetic structure where all the B atoms are equivalent. At low temperatures the Ho cations also take part of the magnetic structure, showing a FM coupling with one of the subsets of moments at the B sublattice. The ordered magnetic moments determined at 2K are 2.33(7) μ_B for Mn/Ru cations and 1.82(8) μ_B for Ho cations. In any case, the low-temperature NPD patterns identified here are clearly distinct from the usual low-T patterns corresponding to pure FM arrangements of the B magnetic moments.[5]

IV. DISCUSSION

The pyrochlore Ho_2MnRuO_7 exhibits a crystallographic structure tightly related to those of the parent $Ho_2Mn_2O_7$ and $Ho_2Ru_2O_7$ oxides. The unit-cell parameter obtained for Ho_2MnRuO_7 [a=10.0491(2) Å], at RT, is in between $Ho_2Mn_2O_7$ (a=9.905 Å) (Ref. 10) and $Ho_2Ru_2O_7$ (a =10.1417 Å).[17] The increment of the cell parameter when the Ru content increases is a result of the higher ionic radii of Ru^{4+} of 0.62 Å, compared to that of Mn^{4+} of 0.53 Å.[22]

Figure 7 shows a schematic view of the different environments of Ho and Mn/Ru cations in Ho_2MnRuO_7. Mn and

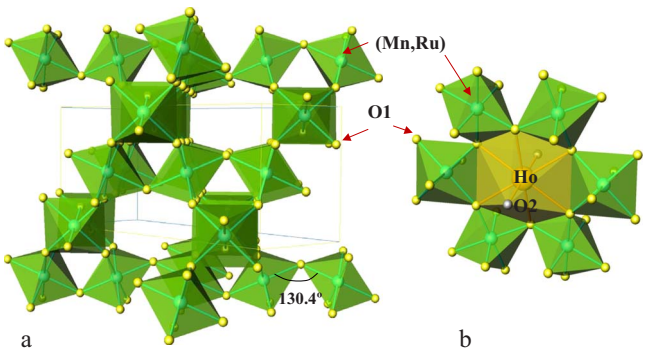

FIG. 7. (Color online) View of the crystallographic structure of Ho_2MnRuO_7 showing (a) the rings of $(Mn,Ru)^{4+}O_6$ octahedra sharing corners and (b) Ho cations eightfold coordinated with oxygens (scalenohedra or distorted cubes).

Ru cations are sixfold coordinated to O1 oxygen atoms at equal distances of 1.9566(7) Å. The B_2O_6 covalent framework of the pyrochlore, constituted by the $(Mn,Ru)O_6$ octahedra sharing corners is shown in Fig. 7(a). In pyrochlore oxides the bond angle B–O–B is close to 130°, in our case it takes the value 130.43°. This arrangement conforms wide cages where A and O2 atoms are located. Ho cations are eightfold coordinated with six O1 oxygen atoms at distances of 2.4533(7) Å (at RT) and with two O2 oxygen atoms at distances of 2.17569(2) Å in a scalenohedron (distorted cube), as highlighted in Fig. 7(b).

Compared to $Ho_2Ru_2O_7$,[16] the distances Ho-O2 and Ru-O1 are smaller in Ho_2MnRuO_7 due to the smaller ionic radii of Mn^{4+} in contrast with that of Ru^{4+}, however, Ho-O1 are longer in Ho_2MnRuO_7. In pyrochlore oxides the shape of the coordination polyhedra of A and B cations is a direct function of the oxygen (O1) u parameter, that is defined as $u=3/4-x$, where x is the atomic parameter for O1 in the considered setting of the space group $Fd\bar{3}m$, with the origin at (1/8, 1/8, 1/8). When $u\sim7/16$ (0.4375) the coordination around B becomes a regular octahedron, and when $u\sim3/8$ (0.375), the coordination around A becomes a regular cube. In our case, at RT x=0.3316(1) and therefore $u=0.4184(1)$ that determines a coordination around B atoms close to a regular octahedron [Fig. 7(a)]. The A–O2–A bond angle is always 109.47° since $(A)_4O2$ groups form regular tetrahedra by the geometry of the space group.

Tables I and II show the evolution of the atomic parameters and the distances of Ho_2MnRuO_7 when the temperature decreases. The unit-cell parameter and the volume decrease as expected from the thermal contraction, and the same effect is observed for the distances.

The magnetism of the parent $Ho_2Mn_2O_7$ and $Ho_2Ru_2O_7$ oxides has been widely studied, although some controversial results have been reported. $Ho_2Mn_2O_7$ presents dominant FM interactions between Mn cations below ~35 K.[23] The FM behavior appears to be the result of the direct Mn–O–Mn superexchange interactions. When this angle is 180° the interactions between Mn are AFM in nature, however, when this angle decreases (~90°) both FM and AFM interactions occur.[24] In the pyrochlore structure this angle is ~130° and one should expect the occurrence of AFM interactions, however, the geometrical frustration intrinsic of the pyrochlore structure prevents the manifestation of a pure AFM long-range ordering. Then, the result is the appearance of weak FM interactions, as observed from the macroscopic magnetic measurements and neutron diffraction experiments, with a strong component of spin-glass behavior. In fact, NPD data shows, only at low temperatures, the presence of a collinear FM coupling between the Mn^{4+} and the Ho^{3+} sublattices.[10,15,23]

On the other hand, $Ho_2Ru_2O_7$ displays two magnetic transitions at T~95 K and T~1.4 K to give long-range ordered states involving the Ru (nearly collinear ferromagnet) and Ho sublattices, respectively. Between these transitions, the Ho^{3+} moments form short-ranged ordered spin clusters. It is suggested that the internal field provided by the ordered Ru^{4+} moments destroys the fragile spin-ice state and drives the Ho^{3+} moments to order.[18]

In Ho_2MnRuO_7, Mn^{4+} ($S=3/2$ spins) and Ru^{4+} ($S=1$ spins) cations are randomly distributed over the 16*c* positions of the structure. The susceptibility curve indicates an ordered magnetic temperature around 65 K, which is in between T_C of $Ho_2Mn_2O_7$ ($T_C \sim 35$ K) and $Ho_2Ru_2O_7$ ($T_C \sim 95$ K). By NPD we observed the establishment of an AFM arrangement between two subsets of atoms at the 16*c* positions. This magnetic arrangement has never been observed in a pyrochlore-like oxide, where the magnetic frustration prevents the consolidation of an AFM long-range ordering. We believe that the random distribution of Mn and Ru cations over the B positions relieves part of the magnetic frustration and makes it possible this long-range arrangement. Below 30 K (Fig. 3), the additional increment of the susceptibility occurs due to the polarization of the Ho^{3+} magnetic moments, which participate in the magnetic structure. In fact, from NPD data we have also determined the ordered magnetic moments over Mn/Ru positions as 2.33(7) μ_B at 2 K, presenting an average value between those expected for Mn^{4+} and Ru^{4+} spins. The reduction with respected the expected value of 2.5 μ_B/atom indicates that the ordering is not complete. The weak ordered moment obtained for Ho positions (1.82(8) μ_B) suggests that, in the absence of a magnetic field, the Ho moments remain at 80% in a paramagnetic state.

However, the application of an external filed is able to fully polarize the Ho moments. The saturation magnetization at 2 K obtained from the hysteresis loop measured for the maximum magnetic field of 5 T is 10.8 μ_B/f.u.. This value has to be contrasted with that expected for free Ho^{3+} (10.0 μ_B), Mn^{4+} (3 μ_B), and Ru^{4+} (2 μ_B) cations. The observed value is very close to that resulting from an AFM coupling between Mn^{4+} and Ru^{4+} moments, which are distributed at random and thus they give a null magnetization at $H=0$ and the full polarization of Ho^{3+} moments.

Below the ordered magnetic temperature, the ZFC curve diverges from the FC curve; this divergence has been usually attributed to a spin-glass like behavior due to geometrical frustration, which is very usual in many pyrochlore oxides.[25–27] As we have commented before, similar features have been reported for both $Ho_2Mn_2O_7$ and $Ho_2Ru_2O_7$ pyrochlores. To investigate this metastable magnetic state we have carried out ac susceptibility measurements. The ac susceptibility presents two peaks as follows: the first one corresponds to the main increase of the dc susceptibility that appears at $T \sim 65$ K, actually corresponding to the long-range ordering temperature involving Mn^{4+} and Ru^{4+} moments. The other peak at $T \sim 30-35$ K, is a strong frequency dependence peak, matching the onset of the ZFC-FC divergence in the dc results. On increasing the frequency, the intensity of the maximum in both curves shifts to higher temperature. This behavior is characteristic of a spin-glass like state.[28]

We have, thus, an hybrid scenario where we observe that the random distribution of Mn and Ru atoms over the B positions of the pyrochlore partially relieve the geometrical frustration inherent to the pyrochlore structure but there is a reminiscent spin-glass effect that also arises from the mentioned random distribution and the FM coupling of Ho moments with the two subsets of opposite moments at the B sites.

V. CONCLUSIONS

Ho_2MnRuO_7 exhibits a conventional pyrochlore structure, with atomic parameters intermediate between those of the parent $Ho_2Mn_2O_7$ and $Ho_2Ru_2O_7$ oxides. This compound shows a magnetic transition at $T \sim 65$ K as shown by dc magnetic susceptibility data, the nature of this ordering was unveiled by a NPD study at 2 and 10 K as an AFM order of two subsets of the Mn/Ru spins at 16*c* sites, indicating that the magnetic frustration is partially relieved by the random distribution of Mn and Ru over these positions, with a partial participation of the Ho^{3+} magnetic moments. The ac data present frequency variability below 60 K and broad frequency dependent maxima at lower temperatures (~ 30 K), suggesting a spin-glass like behavior similar to $Ho_2Mn_2O_7$. Under an external magnetic field the Ho moments become totally polarized, giving a saturation magnetization at 2 K of 10.8 μ_B/f.u. at 5 T.

ACKNOWLEDGMENTS

We thank the financial support of the Spanish Ministry of Education to the projects Grant Nos. MAT2007-60536 and MAT2008-06517-C02-01 and we are grateful to the Institut Laue-Langevin (ILL) for making all facilities available.

[1] M. A. Subramanian, G. Aravamudan, and G. V. Subba Rao, Prog. Solid State Chem. **15**, 55 (1983).
[2] Y. Shimakawa, Y. Kubo, and T. Manako, Nature (London) **379**, 53 (1996).
[3] Y. Shimakawa, Y. Kubo, T. Manako, Y. V. Sushko, D. N. Argyriou, and J. D. Jorgensen, Phys. Rev. B **55**, 6399 (1997).
[4] M. A. Subramanian, B. H. Toby, A. P. Ramirez, W. J. Marshall, A. W. Sleight, and G. H. Kewi, Science **273**, 81 (1996).
[5] J. A. Alonso, M. J. Martínez-Lope, M. T. Casais, J. L. Martínez, and M. T. Fernández-Díaz, Chem. Mater. **12**, 1127 (2000).
[6] J. A. Alonso, J. L. Martínez, M. J. Martínez-Lope, M. T. Casais, and M. T. Fernández-Díaz, Phys. Rev. Lett. **82**, 189 (1999).
[7] J. A. Alonso, P. Velasco, M. J. Martínez-Lope, M. T. Casais, J. L. Martínez, M. T. Fernández-Díaz, and J. M. de Paoli, Appl. Phys. Lett. **76**, 3274 (2000).
[8] J. A. Alonso, M. J. Martínez-Lope, M. T. Casais, P. Velasco, J. L. Martínez, M. T. Fernández-Díaz, and J. M. de Paoli, Phys. Rev. B **60**, R15024 (1999).
[9] D.-K. Seo, M.-H. Whangbo, and M. A. Subramanian, Solid State Commun. **101**, 417 (1997).
[10] M. A. Subramanian, C. C. Torardi, D. C. Johnson, J. Pannetier, and A. W. Sleight, J. Solid State Chem. **72**, 24 (1988).
[11] J. E. Greedan, J. Avelar, and M. A. Subramanian, Solid State Commun. **82**, 797 (1992).
[12] J. E. Greedan, N. P. Raju, and M. A. Subramanian, Solid State Commun. **99**, 399 (1996).
[13] Y. Shimakawa, Y. Kudo, N. Hamada, J. D. Jorgensen, Z. Hu, S. Short, M. Nohara, and H. Takagi, Phys. Rev. B **59**, 1249 (1999).
[14] J. N. Reimers, J. E. Greedan, R. K. Kremer, E. Gmelin, and M. A. Subramanian, Phys. Rev. B **43**, 3387 (1991).
[15] J. E. Greedan, N. P. Raju, A. Maignan, C. Simon, J. S. Pedersen, A. M. Niraimathi, E. Gmelin, and M. A. Subramanian, Phys. Rev. B **54**, 7189 (1996).
[16] M. Sato and Y. Suzumura, J. Phys. Chem. Solids **62**, 1 (2001).
[17] C. Bansal, H. Kawanaka, H. Bando, and Y. Nishihara, Phys. Rev. B **66**, 052406 (2002).
[18] C. R. Wiebe, J. S. Gardner, S. J. Kim, G. M. Luke, A. S. Wills, B. D. Gaulin, J. E. Greedan, I. Swainson, Y. Qiu, and C. Y. Jones, Phys. Rev. Lett. **93**, 076403 (2004).

[19]J. P. Clancy, J. P. C. Ruff, S. R. Dunsiger, Y. Zhao, H. A. Dabkowska, J. S. Gardner, Y. Qiu, J. R. D. Copley, T. Jenkins, and B. D. Gaulin, Phys. Rev. B **79**, 014408 (2009).
[20]H. M. Rietveld, J. Appl. Crystallogr. **2**, 65 (1969).
[21]J. Rodríguez-Carvajal, Physica B **192**, 55 (1993).
[22]R. D. Shannon, Acta Crystallogr., Sect. A: Cryst. Phys., Diffr., Theor. Gen. Crystallogr. **32**, 751 (1976).
[23]N. P. Raju, J. E. Greedan, J. S. Pedersen, C. Simon, A. Maignan, and M. A. Subramanian, J. Appl. Phys. **79**, 6173 (1996).
[24]J. B. Goodenough, *Magnetism and The Chemical Bond* (Wiley, New York, 1966), p. 181.
[25]M. J. Harris, S. T. Bramwell, D. F. McMorrow, T. Zeiske, and K. W. Godfrey, Phys. Rev. Lett. **79**, 2554 (1997).
[26]S. T. Bramwell and M. J. P. Gingras, Science **294**, 1495 (2001).
[27]J. E. Greedan, J. Mater. Chem. **11**, 37 (2001).
[28]J. A. Mydosh, *Spin Glasses* (Taylor & Francis, London, 1993).